Supplementary material for "Entanglement-interference complementarity and experimental demonstration in a superconducting circuit"

Xin-Jie Huang[1,*] Pei-Rong Han[1,*] Wen Ning[1], Shou-Bang Yang[1], Xin Zhu[1], Jia-Hao Lü[1], Ri-Hua Zheng[1], Hekang Li[2], Zhen-Biao Yang[1,†] Kai Xu[2,3], Chui-Ping Yang[4,5,‡] Qi-Cheng Wu[5], Dongning Zheng[2,3], Heng Fan[2,3], and Shi-Biao Zheng[1§]

1.Fujian Key Laboratory of Quantum Information and Quantum Optics, College of Physics and Information Engineering, Fuzhou University, Fuzhou, Fujian 350108, China

2.Institute of Physics, Chinese Academy of Sciences, Beijing 100190,China

3.CAS Center for Excellence in Topological Quantum Computation, Beijing 100190, China

4.School of Physics, Hangzhou Normal University, Hangzhou 311121, China and

5.Quantum Information Research Center, Shangrao Normal University, Shangrao 334001, China

(Dated: October 8, 2022)

CONTENTS

SYSTEM-WPD CONCURRENCE

When the coherence between the two paths is partially lost before the qubit-WPD coupling due to dephasing, the joint state of this qubit and the WPD after their coupling (Eq. (8) of the main text) can be rewritten as

$$\begin{aligned}\rho \;=\; \frac{1}{2}\Bigg[&|0\rangle\langle 0| \otimes |W_0\rangle\langle W_0| + |1\rangle\langle 1| \otimes \left(V_0 e^{i\phi}|W_0\rangle + \sqrt{1-V_0^2}|W_1\rangle\right)\left(\langle W_0|V_0 e^{-i\phi} + \langle W_1|\sqrt{1-V_0^2}\right)\\ &+iC_0 e^{-i\theta}|0\rangle\langle 1| \otimes |W_0\rangle\left(\langle W_0|V_0 e^{-i\phi} + \langle W_1|\sqrt{1-V_0^2}\right)\\ &-iC_0 e^{i\theta}|1\rangle\langle 0| \otimes \left(V_0 e^{i\phi}|W_0\rangle + \sqrt{1-V_0^2}|W_1\rangle\right) \otimes \langle W_0|\Bigg],\end{aligned} \tag{S1}$$

where $V_0 = |\langle W_0|U|W_0\rangle|$ and $\phi = \arg\left(\langle W_0|U|W_0\rangle\right)$. In the joint qubit-WPD basis $\{|0\rangle|W_0\rangle, |0\rangle|W_1\rangle, |1\rangle|W_0\rangle, |1\rangle|W_1\rangle\}$, ρ can be expressed in the matrix form

$$\rho = \frac{1}{2}\begin{pmatrix} 1 & 0 & iC_0V_0e^{-i(\theta+\phi)} & iC_0\sqrt{1-V_0^2}e^{-i\theta} \\ 0 & 0 & 0 & 0 \\ -iC_0V_0e^{i(\theta+\phi)} & 0 & V_0^2 & V_0\sqrt{1-V_0^2}e^{i\phi} \\ -iC_0\sqrt{1-V_0^2}e^{i\theta} & 0 & V_0\sqrt{1-V_0^2}e^{-i\phi} & 1-V_0^2 \end{pmatrix}. \tag{S2}$$

The entanlgement between the interfering qubit and the WPD is determined by the eigenvalues of the operator $\widetilde{\rho} = \rho\left(\sigma_{q,y}\otimes\sigma_{w,y}\right)\rho^*\left(\sigma_{q,y}\otimes\sigma_{w,y}\right)$, where $\sigma_{q,y}$ and $\sigma_{w,y}$ are the y-components of the Pauli operator for the qubit and the WPD, respectively. The matrix $\widetilde{\rho}$ reads as

$$\widetilde{\rho} = \frac{1}{4}\begin{pmatrix} \left(1+C_0^2\right)\left(1-V_0^2\right) & -V_0\sqrt{1-V_0^2}\left(1+C_0^2\right)e^{i\phi} & 0 & 2iC_0\sqrt{1-V_0^2}e^{-i\theta} \\ 0 & 0 & 0 & 0 \\ -2iV_0\left(1-V_0^2\right)C_0e^{i(\phi+\theta)} & 2iV_0^2\sqrt{1-V_0^2}C_0e^{i(2\phi+\theta)} & 0 & V_0\sqrt{1-V_0^2}\left(1+C_0^2\right)e^{i\phi} \\ -2i\left(1-V_0^2\right)^{3/2}C_0e^{i\theta} & 2iV_0\sqrt{1-V_0^2}C_0e^{i(\phi+\theta)} & 0 & \left(1+C_0^2\right)\left(1-V_0^2\right) \end{pmatrix}. \tag{S3}$$

The four eigenvalues of $\widetilde{\rho}$ in the decreasing order are respectively $\lambda_1 = \frac{1}{4}\left(1-V_0^2\right)\left(1+C_0\right)^2$, $\lambda_2 = \frac{1}{4}\left(1-V_0^2\right)\left(1-C_0\right)^2$ and $\lambda_3 = \lambda_4 = 0$. The corresponding concurrence [1], defined as $C = \max\{\sqrt{\lambda_1}-\sqrt{\lambda_2}-\sqrt{\lambda_3}-\sqrt{\lambda_4}, 0\}$, is $C_0\sqrt{1-V_0^2}$.

For the unbalanced interferometer where the two paths are not equally populated, the corresponding qubit's state before interaction with the WPD can be described by the density operator

$$\rho_{q,0} = \cos^2\alpha|0\rangle\langle 0| + \cos^2\alpha|1\rangle\langle 1| + \frac{i}{2}C_0\left(e^{-i\theta}|0\rangle\langle 1| - e^{i\theta}|1\rangle\langle 0|\right). \tag{S4}$$

After the qubit-WPD coupling, the total density operator is

$$\begin{aligned} \rho \; = \; & \cos^2\alpha|0\rangle\langle 0|\otimes|W_0\rangle\langle W_0| + \sin^2\alpha|1\rangle\langle 1|\otimes\left(V_0e^{i\phi}|W_0\rangle + \sqrt{1-V_0^2}|W_1\rangle\right)\left(\langle W_0|V_0e^{-i\phi} + \langle W_1|\sqrt{1-V_0^2}\right) \\ & + \frac{i}{2}C_0e^{-i\theta}|0\rangle\langle 1|\otimes|W_0\rangle\left(\langle W_0|V_0e^{-i\phi} + \langle W_1|\sqrt{1-V_0^2}\right) \\ & - \frac{i}{2}C_0e^{i\theta}|1\rangle\langle 0|\otimes\left(V_0e^{i\phi}|W_0\rangle + \sqrt{1-V_0^2}|W_1\rangle\right)\otimes\langle W_0|\Bigg], \end{aligned} \tag{S5}$$

which can be rewritten as

$$\rho = \begin{pmatrix} \cos^2\alpha & 0 & \frac{i}{2}C_0V_0e^{-i(\theta+\phi)} & \frac{i}{2}C_0\sqrt{1-V_0^2}e^{-i\theta} \\ 0 & 0 & 0 & 0 \\ -\frac{i}{2}\sin^2\alpha C_0V_0e^{i(\theta+\phi)} & 0 & \sin^2\alpha V_0^2 & \sin^2\alpha V_0\sqrt{1-V_0^2}e^{i\phi} \\ -\frac{i}{2}\sin^2\alpha C_0\sqrt{1-V_0^2}e^{i\theta} & 0 & \sin^2\alpha V_0\sqrt{1-V_0^2}e^{-i\phi} & \sin^2\alpha\left(1-V_0^2\right) \end{pmatrix}. \tag{S6}$$

The corresponding $\widetilde{\rho}$ matrix is given by

$$\widetilde{\rho} = \begin{pmatrix} \frac{1}{4}\left(C_0^2+\sin^2 2\alpha\right)\left(1-V_0^2\right) & -\frac{1}{4}V_0\sqrt{1-V_0^2}\left(\sin^2 2\alpha + C_0^2\right)e^{i\phi} & 0 & i\cos^2\alpha C_0\sqrt{1-V_0^2}e^{-i\theta} \\ 0 & 0 & 0 & 0 \\ -i\sin^2\alpha V_0\left(1-V_0^2\right)C_0e^{i(\phi+\theta)} & i\sin^2\alpha V_0^2\sqrt{1-V_0^2}C_0e^{i(2\phi+\theta)} & 0 & \frac{1}{4}V_0\sqrt{1-V_0^2}\left(\sin^2 2\alpha + C_0^2\right)e^{i\phi} \\ -i\sin^2\alpha\left(1-V_0^2\right)^{3/2}C_0e^{i\theta} & i\sin^2\alpha V_0\sqrt{1-V_0^2}C_0e^{i(\phi+\theta)} & 0 & \frac{1}{4}\left(\sin^2 2\alpha + C_0^2\right)\left(1-V_0^2\right) \end{pmatrix}. \tag{S7}$$

The four eigenvalues of $\widetilde{\rho}$ in the decreasing order are respectively $\lambda_1 = \frac{1}{4}\left(1-V_0^2\right)\left(\sin 2\alpha + C_0\right)^2$, $\lambda_2 = \frac{1}{4}\left(1-V_0^2\right)\left(\sin 2\alpha - C_0\right)^2$ and $\lambda_3 = \lambda_4 = 0$. The corresponding concurrence, defined as $C = \max\{\sqrt{\lambda_1}-\sqrt{\lambda_2}-\sqrt{\lambda_3}-\sqrt{\lambda_4}, 0\}$, is also equal to $C_0\sqrt{1-V_0^2}$.

FRINGE CONTRAST

After the second Hadamard transformation on the interfering qubit, the total density operator is

$$\begin{aligned}\rho \;=\; & \frac{1}{2}\cos^2\alpha\left(|0\rangle - i|1\rangle\right)\left(\langle 0| + \langle 1|i\right)\otimes|W_0\rangle\langle W_0| \\ & +\frac{1}{2}\sin^2\alpha\left(|1\rangle - i|0\rangle\right)\left(\langle 1| + \langle 0|i\right)\otimes\left(V_0e^{i\phi}|W_0\rangle + \sqrt{1-V_0^2}|W_1\rangle\right)\left(\langle W_0|V_0e^{-i\phi} + \langle W_1|\sqrt{1-V_0^2}\right) \\ & +\frac{i}{4}C_0e^{-i\theta}\left(|0\rangle - i|1\rangle\right)\left(\langle 1| + \langle 0|i\right)\otimes|W_0\rangle\left(\langle W_0|V_0e^{-i\phi} + \langle W_1|\sqrt{1-V_0^2}\right) \\ & -\frac{i}{4}C_0e^{i\theta}\left(|1\rangle - i|0\rangle\right)\left(\langle 0| + \langle 1|i\right)\otimes\left(V_0e^{i\phi}|W_0\rangle + \sqrt{1-V_0^2}|W_1\rangle\right)\otimes\langle W_0|\Bigg].\end{aligned} \tag{S8}$$

Tracing over the degree of freedom of the WPD, we obtain the reduced density operator of the interfering qubit

$$\begin{aligned}\rho_q \;=\; & \frac{1}{2}\cos^2\alpha\left(|0\rangle - i|1\rangle\right)\left(\langle 0| + \langle 1|i\right) \\ & +\frac{1}{2}\sin^2\alpha\left(|1\rangle - i|0\rangle\right)\left(\langle 1| + \langle 0|i\right) \\ & +\frac{i}{4}C_0V_0e^{-i(\theta+\phi)}\left(|0\rangle - i|1\rangle\right)\left(\langle 1| + \langle 0|i\right) \\ & -\frac{i}{4}C_0V_0e^{-i(\theta+\phi)}\left(|1\rangle - i|0\rangle\right)\left(\langle 0| + \langle 1|i\right)\Bigg].\end{aligned} \tag{S9}$$

The probability of detecting the qubit in the state $|1\rangle$ is

$$P_1 = \langle 1|\rho_q|1\rangle = \frac{1}{2}\left[1 + C_0V_0\cos\left(\theta+\phi\right)\right]. \tag{S10}$$

Therefore, the fringe contrast is also given by C_0V_0.

DISTINGUISHABILITY

The amount of the which-path information stored in the WPD, is quantified by the distinguishability, defined as [2]

$$D = \frac{1}{2}\mathrm{tr}_w|\rho_{w,0} - \rho_{w,1}|, \tag{S11}$$

where $\rho_{w,0}$ and $\rho_{w,1}$ respectively denote the density operators of the WPD associated with the interfering qubit's $|0\rangle$ and $|1\rangle$ states after their coupling, given by

$$\rho_{w,0} \;=\; \langle 0|\rho|0\rangle/\mathrm{tr}_w\left(\langle 0|\rho|0\rangle\right) = |W_0\rangle\langle W_0|, \tag{S12}$$

$$\begin{aligned}\rho_{w,1} \;=\; & \langle 1|\rho|1\rangle/\mathrm{tr}_w\left(\langle 0|\rho|0\rangle\right) = \left(V_0e^{i\phi}|W_0\rangle + \sqrt{1-V_0^2}|W_1\rangle\right) \\ & \otimes\left(\langle W_0|V_0e^{-i\phi} + \langle W_1|\sqrt{1-V_0^2}\right).\end{aligned} \tag{S13}$$

In the basis $\{|W_0\rangle, |W_1\rangle\}$, $\rho_{w,0} - \rho_{w,1}$ is given by the matrix

$$\begin{pmatrix} 1-V_0^2 & -V_0\sqrt{1-V_0^2}e^{i\phi} \\ -V_0\sqrt{1-V_0^2}e^{-i\phi} & V_0^2-1 \end{pmatrix}. \tag{S14}$$

The two eigenvalues of $\rho_{w,0} - \rho_{w,1}$ are

$$\lambda_\pm = \pm\sqrt{1-V_0^2}. \tag{S15}$$

Therefore, the distinguishability is

$$D = \frac{1}{2}\left(|\lambda_+| + |\lambda_-|\right) = \sqrt{1-V_0^2}, \tag{S16}$$

which is equal to the qubit-WPD concurrence only when $C_0 = 1$.

IMPLEMENTATION OF THE DYNAMIC MODEL WITH ADDITIONAL PHASES

Single qubit rotation

A rotation around the axis

$$\vec{n} = \left(\sin\tilde{\theta}\cos\phi, \sin\tilde{\theta}\sin\phi, \cos\tilde{\theta}\right), \tag{S17}$$

in which $\tilde{\theta}$ is the polar angle and ϕ is the equatorial angle, by an angle γ, can be written as a rotation operator

$$R_{\gamma}^{\vec{n}} = \begin{pmatrix} \cos\frac{\gamma}{2} - i\sin\frac{\gamma}{2}\cos\tilde{\theta} & -i\sin\frac{\gamma}{2}\sin\tilde{\theta}e^{-i\phi} \\ -i\sin\frac{\gamma}{2}\sin\tilde{\theta}e^{i\phi} & \cos\frac{\gamma}{2} + i\sin\frac{\gamma}{2}\cos\tilde{\theta} \end{pmatrix}. \tag{S18}$$

We choose

$$\tilde{\theta} = \frac{\pi}{2}\left(\tilde{\theta} = \frac{\pi}{2}\right), \tag{S19}$$

$$\phi = \theta\left(\phi = -\omega_r\frac{\pi}{2g_2}\right), \tag{S20}$$

$$\gamma = \frac{\pi}{2}\left(\gamma = \frac{\pi}{2}\right), \tag{S21}$$

and apply this rotation operator to qubit Q_1 (Q_2). Thus we have

$$\begin{aligned} R_{\frac{\pi}{2}}^{\vec{n}_1}|0_1\rangle &= \frac{1}{\sqrt{2}}\begin{pmatrix} 1 - i\cos\tilde{\theta} & -i\sin\tilde{\theta}e^{-i\phi} \\ -i\sin\tilde{\theta}e^{i\phi} & 1+\cos\tilde{\theta} \end{pmatrix}\begin{pmatrix} 1 \\ 0 \end{pmatrix} \\ &\equiv \frac{1}{\sqrt{2}}\left[|0_1\rangle - ie^{i\theta}|1_1\rangle\right], \end{aligned} \tag{S22}$$

$$R_{\frac{\pi}{2}}^{\vec{n}_2}|0_2\rangle = \frac{1}{\sqrt{2}}\left[|0_2\rangle - ie^{-i\omega_r\frac{\pi}{2g_2}}|1_2\rangle\right]. \tag{S23}$$

The phase factor $\phi = -\omega_r\frac{\pi}{2g_2}$ is chosen to cancel the relative phase induced during the resonant Q_2-R interaction. The sum of the modulus of the off-diagonal elements of

$$R_{\frac{\pi}{2}}^{\vec{n}_1}|0_1\rangle\langle 0_1|R_{\frac{\pi}{2}}^{\vec{n}_1+} = \frac{1}{2}\begin{pmatrix} 1 & ie^{-i\theta} \\ -ie^{i\theta} & 1 \end{pmatrix} \tag{S24}$$

characterizes the coherence, that is

$$C_0 = |\frac{1}{2}ie^{-i\theta}| + | -\frac{1}{2}ie^{i\theta}| = 1, \tag{S25}$$

between the two paths.

Q_1-resonator interaction

Once the Q_2-R interaction stops, we tune Q_2 back to its idle frequency and adjust Q_1 to its working frequency to start the Q_1-R interaction, for which only the qubit's transition $|1\rangle \leftrightarrow |2\rangle$ is involved while the other transitions are decoupled. The ideal model describing the interaction is written as:

$$H_{Q_1R}/\hbar = \omega_1|1\rangle\langle 1| + \omega_2|2\rangle\langle 2| + \omega_r a^+a + \sqrt{2}g_1\left(a^+|1\rangle\langle 2| + a|2\rangle\langle 1|\right), \tag{S26}$$

where $\hbar\omega_2$ ($\hbar\omega_1$) is the energy level for the Q_1's $|2\rangle$ ($|1\rangle$) state. In the single-excitation subspace $\{|2\rangle|0_r\rangle, |1\rangle|1_r\rangle\}$, Eq. (S26) possesses two eigenstates

$$|\phi_\pm\rangle = N_\pm^{-1}\left[2\sqrt{2}g_1|1\rangle|1_r\rangle + (\delta \pm 2\Omega)|2\rangle|0_r\rangle\right], \tag{S27}$$

where $N_\pm = \sqrt{(\delta^2 \pm 2\Omega)^2 + 8g_1^2}$ are the normalization factors, $\delta = \omega_2 - \omega_1 - \omega_r$ and $\Omega = \sqrt{2g_1^2 + \delta^2/4}$. The corresponding eigenenergies for (S27) are

$$E_\pm = \hbar(2\omega_2 - \delta)/2 \pm \hbar\Omega. \tag{S28}$$

The temporal evolution of the initial qubit-resonator state $|\Psi'(0)\rangle = |1\rangle|1_r\rangle$ can be expressed as

$$\begin{aligned}
|\Psi(t)\rangle &= e^{-iH_{Q_1R}t/\hbar}|\Psi(0)\rangle \equiv e^{-iH_{Q_1R}t/\hbar}\frac{1}{8\sqrt{2}g_1\Omega}\left[N_-(\delta+2\Omega)|\phi_-\rangle - N_+(\delta-2\Omega)|\phi_+\rangle\right] \\
&= \frac{1}{8\sqrt{2}g_1\Omega}\left[N_-(\delta+2\Omega)e^{-iE_-t}|\phi_-\rangle - N_+(\delta-2\Omega)e^{-iE_+t}|\phi_+\rangle\right] \\
&= e^{-i\frac{2\omega_2-\delta}{2}t}\left\{\left[cos(\Omega t) + i\frac{\delta}{2\Omega}sin(\Omega t)\right]|1\rangle|1_r\rangle - i\frac{\sqrt{2}g_1}{\Omega}sin(\Omega t)|2\rangle|0_r\rangle\right\},
\end{aligned} \tag{S29}$$

which at $t = \pi/\Omega$ reaches

$$|\Psi(\pi/\Omega)\rangle = e^{i\pi\left(1-\frac{2\omega_2-\delta}{2\Omega}\right)}|1\rangle|1_r\rangle. \tag{S30}$$

In the other words, the resonator undergoes an evolution conditional on Q_1' state $|1\rangle$, i.e.,

$$U = e^{i\beta|1_r\rangle\langle 1_r|}, \tag{S31}$$

with the corresponding phase factor

$$\beta = \pi\left(1 - \frac{2\omega_2 - \delta}{2\Omega}\right). \tag{S32}$$

In the rotating frame $H = (\omega_1 + \omega_r)(|1\rangle|1_r\rangle + |2\rangle|0_r\rangle)$, the conditional phase reads

$$\beta = \pi\left[1 - \delta/(2\Omega)\right], \tag{S33}$$

as presented in the main text.

Now, if we start from the initial qubit-resonator state:

$$|\Psi'(0)\rangle = \frac{1}{\sqrt{2}}\left(|0\rangle - ie^{i\theta}|1\rangle\right)|W_0\rangle, \tag{S34}$$

after the qubit-resonator coupling for an interaction time $t = \frac{\pi}{\Omega}$, we get

$$|\Psi'(\pi/\Omega)\rangle = \frac{1}{\sqrt{2}}\left[|0\rangle\frac{1}{\sqrt{2}}\left(|0_r\rangle - e^{-i\omega_r\frac{\pi}{\Omega}}|1_r\rangle\right) - ie^{i\theta}|1\rangle\frac{1}{\sqrt{2}}\left(e^{-i\omega_1\frac{\pi}{\Omega}}|0_r\rangle - e^{i\beta}|1\rangle_r\right)\right], \tag{S35}$$

which can be rewritten as

$$\begin{aligned}
|\Psi'(\pi/\Omega)\rangle &= \frac{1}{\sqrt{2}}\left[|0\rangle\frac{1}{\sqrt{2}}\left(|0_r\rangle - e^{-i\omega_r\frac{\pi}{\Omega}}|1_r\rangle\right) - ie^{i\theta}e^{-i\omega_1\frac{\pi}{\Omega}}|1\rangle\frac{1}{\sqrt{2}}\left(|0_r\rangle - e^{i\left(\beta+\omega_1\frac{\pi}{\Omega}\right)}|1_r\rangle\right)\right] \\
&= \frac{1}{\sqrt{2}}\left[|0\rangle|W_0'\rangle - ie^{i\left(\theta-\omega_1\frac{\pi}{\Omega}\right)}|1\rangle U'|W_0'\rangle\right],
\end{aligned} \tag{S36}$$

where we define

$$|W_0'\rangle = \frac{1}{\sqrt{2}}\left(|0_r\rangle - e^{-i\omega_r\frac{\pi}{\Omega}}|1_r\rangle\right), \tag{S37}$$

$$U' = e^{i\beta'|1_r\rangle\langle 1_r|}, \tag{S38}$$

$$\beta' = \beta + \omega_1\frac{\pi}{\Omega} + \omega_r\frac{\pi}{\Omega}. \tag{S39}$$

The second Hadamard operation

The dynamics for the Hadamard operation is modelled by the interaction Hamiltonian

$$H_q = \frac{1}{2}\hbar\varepsilon e^{i\varphi}|1\rangle\langle 0| + h.c, \tag{S40}$$

where ε, φ and t denote the amplitude, phase and delay of the driving pulse, respectively. Eq. (S40) leads to the following state evolutions

$$|0\rangle \rightarrow cos(\frac{\varepsilon}{2}t)|0\rangle - ie^{i\varphi}sin(\frac{\varepsilon}{2}t)|1\rangle, \tag{S41}$$

$$|1\rangle \rightarrow cos(\frac{\varepsilon}{2}t)|1\rangle - ie^{-i\varphi}sin(\frac{\varepsilon}{2}t)|0\rangle. \tag{S42}$$

The Hadamard operation is given by $R^{\vec{x}}_{\frac{\pi}{2}}$, which is a single qubit rotation around the x-axis by an angle $\pi/2$, corresponding to the transformation ($\varphi = 0$, $\varepsilon t = \pi/2$)

$$|0\rangle \rightarrow (|0\rangle - i|1\rangle)/\sqrt{2}, \tag{S43}$$

$$|1\rangle \rightarrow (|1\rangle - i|0\rangle)/\sqrt{2}. \tag{S44}$$

After the second Hadamard operation, the state, i.e., Eq. (S36), of the Q_1-R coupled system becomes

$$\begin{aligned} R^{\vec{x}}_{\frac{\pi}{2}}|\Psi'(\pi/\Omega)\rangle &= \frac{1}{2}\left[(|0\rangle - i|1\rangle)|W_0'\rangle - ie^{i\left(\theta-\omega_1\frac{\pi}{\Omega}\right)}(|1\rangle - i|0\rangle)U'|W_0'\rangle\right] \\ &= \frac{1}{2}\left[|0\rangle\left(|W_0'\rangle - e^{i\left(\theta-\omega_1\frac{\pi}{\Omega}\right)}U'|W_0'\rangle\right) - i|1\rangle\left(|W_0'\rangle + e^{i\left(\theta-\omega_1\frac{\pi}{\Omega}\right)}U'|W_0'\rangle\right)\right]. \end{aligned} \tag{S45}$$

With Eq. (S45), we can deduce that the probability of detecting Q_1 in the state $|1\rangle$ is

$$\begin{aligned} P_1' &= \frac{1}{4}\left(\langle W_0'| + e^{-i\left(\theta-\omega_1\frac{\pi}{\Omega}\right)}\langle W_0'|U'^{+}\right)\left(|W_0'\rangle + e^{i\left(\theta-\omega_1\frac{\pi}{\Omega}\right)}U'|W_0'\rangle\right) \\ &= \frac{1}{4}\left(1 + e^{-i\left(\theta-\omega_1\frac{\pi}{\Omega}\right)}\langle W_0'|U'^{+}|W_0'\rangle + e^{i\left(\theta-\omega_1\frac{\pi}{\Omega}\right)}\langle W_0'|U'|W_0'\rangle + 1\right) \\ &= \frac{1}{2}\left[1 + V_0'\cos\left(\theta + \phi' - \omega_1\frac{\pi}{\Omega}\right)\right], \end{aligned} \tag{S46}$$

where $V_0' = |\langle W_0'|U'|W_0'\rangle|$ and $\phi' = arg(\langle W_0'|U'|W_0'\rangle)$.

DEVICE PARAMETERS AND EXPERIMENTAL SETUP

Our device consists of five frequency-tunable superconducting Xmon qubits, with the anharmonicities being about $\alpha_j \simeq 2\pi \times 240$ MHz. Each qubit has a microwave line (XY line) for driving its state transition, and an individual flux line (Z line) for dynamically tuning its frequency [3, 4], allowing its flexible coupling (with the strength g_j) to the bus resonator, whose bare frequency and energy relaxation time are $\omega_r/2\pi \simeq 5.582\,\mathrm{GHz}$ and $T_r \simeq 13\ \mu$s (see TABLE.S1), respectively [3, 5–7]. Besides, each qubit is dispersively coupled to its own readout resonator, whose frequency and leakage rate are $\omega_{re,j}/2\pi$ and $\kappa_{r,j}$, respectively. All the readout resonators couple to a common transmission line for multiplexed readout of all qubits' states. The readout is the type of single-shot measurement and is achieved with assistance of an impedance-transformed Josephson parametric amplifier (JPA) with bandwidth of about 150 MHz used to strength the signal-to-noise ratio. The two qubits chosen in the experiment, are marked as Q_1 and Q_2, whose properties are characterized and listed in TABLE.S1. Qubits' s energy relaxation time $T_{1,j}^{|k\rangle}$ (j and k indicate the qubit and its state, respectively), the Ramsey Gaussian dephasing time $T_{2,j}^{*,|k\rangle}$, and the spin echo Gaussian dephasing time $T_{2,j}^{SE,|k\rangle}$ are measured at their idle frequency $\omega_{id}^{|1\rangle}/2\pi$. The probability of correctly reading out each qubit (Q_j) in state $|k\rangle$ is $F_{k,j}$.

Parameters	Q_1	Q_2
Qubit's idle frequency, $\omega_{id}^{\|1\rangle}/2\pi$	5.967 GHz	5.354 GHz
Readout frequency, $\omega_{re,j}/2\pi$	6.850 GHz	6.764 GHz
Coupling strength to the bus resonator, $g_j/2\pi$	19.2 MHz ($\|0\rangle \leftrightarrow \|1\rangle$)	19.9 MHz ($\|0\rangle \leftrightarrow \|1\rangle$)
Energy relaxation time, $T_{1,j}^{\|1\rangle}$ ($T_{1,j}^{\|2\rangle}$)	17.1 (7.6) µs	23.4 (14.7) µs
Ramsey dephasing time, $T_{2,j}^{\star,\|1\rangle}$ ($T_{2,j}^{\star,\|2\rangle}$)	3.0 (2.3) µs	2.4 (2.2) µs
Dephasing time with spin echo, $T_{2,j}^{SE,\|1\rangle}$ ($T_{2,j}^{SE,\|2\rangle}$)	5.7 (4.7) µs	6.5 (3.2) µs
Leakage rate of readout resonator, $\kappa_{r,j}$	1/(313 ns)	1/(315 ns)
Nonlinearity, $\alpha_j/2\pi$	241 MHz	240 MHz
$\|0\rangle$ state readout fidelity, $F_{0,j}$	0.9930	0.9803
$\|1\rangle$ state readout fidelity, $F_{1,j}$	0.8917	0.9073
$\|2\rangle$ state readout fidelity, $F_{2,j}$	0.8483	0.8890

TABLE S1. **Qubits characteristics.** In the experiment, both qubits are initialized to the ground state $|0\rangle$ at their respective idle frequencies $\omega_{id,j}/2\pi$, at which point the listed qubit' coherence parameters (including the lifetime $T_{1,j}^{|k\rangle}$, the Ramsey Gaussian dephasing time $T_{2,j}^{*,|k\rangle}$, and the spin echo Gaussian dephasing time $T_{2,j}^{SE,|k\rangle}$) are measured. $\omega_{id,j}$ is also the point at which single-qubit rotations and state tomographies are performed. g_1 (g_2) is the coupling strength between Q_1 (Q_2) and the bus resonator, achieved by measurement of Rabi oscillation between Q_1's $|1\rangle \leftrightarrow |2\rangle$ (Q_2's $|0\rangle \leftrightarrow |1\rangle$) transition and the bus resonator's photon. The detuning between the qubit's $|1\rangle \leftrightarrow |2\rangle$ and $|0\rangle \leftrightarrow |1\rangle$ transitions gives the qubit's anharmonicity α_j. The fidelity for correctly measuring each qubit's state is $F_{j,k}$, characterized by extracting information of each readout resonator, whose frequency and leakage rate are $\omega_{re,j}/2\pi$ and κ_r, respectively.

When the bias pulse tunes the qubit frequency exactly on resonance with the resonator, through either $|1\rangle \leftrightarrow |2\rangle$ or $|0\rangle \leftrightarrow |1\rangle$ transition, the vacuum Rabi swaps between the qubit and the resonator have the largest amplitude and the longest duration. The coupling strength can be characterized by fitting the oscillation of P_2 (P_1) versus the evolution time at a fixed frequency. Fig. S1 shows the swap spectroscopy for Q_1 and Q_2 by sweeping the bias amplitude and the evolution time. Another spectroscopy measurement is implemented to characterize the qubit frequency as a function of the bias, as shown in Fig. S2. The avoided crossing at the resonant point indicates that the coupling strength between Q_1's $|1\rangle \leftrightarrow |2\rangle$ transition and the resonator is $2\pi \times 27.1$ GHz.

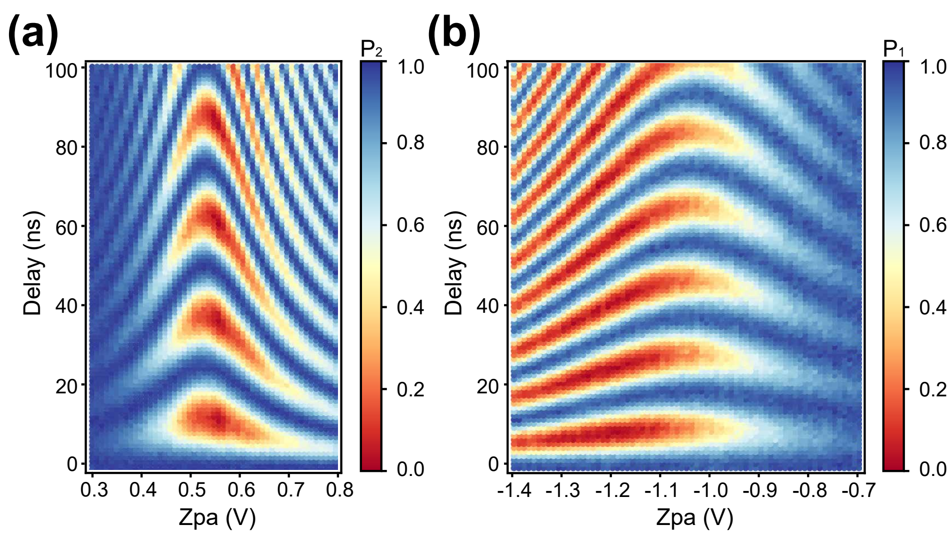

FIG. S1. Vacuum Rabi swap spectroscopy. (a) The swapping between Q_2's $|1\rangle|0_r\rangle \leftrightarrow |0\rangle|1_r\rangle$ transition and the resonator. (b) The swapping between Q_1's $|2\rangle|0_r\rangle \leftrightarrow |1\rangle|1_r\rangle$ transition and the resonator.

The experimental setup where the whole electronics and wiring for the device control is outlined and shown in Fig.

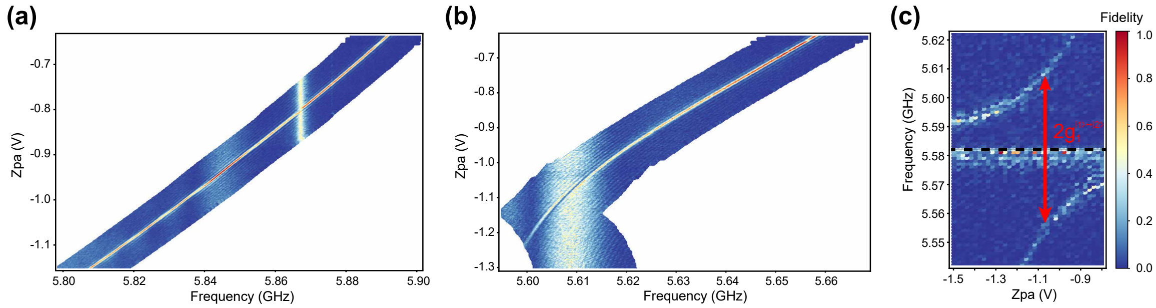

FIG. S2. The qubit spectroscopy. (a) Spectroscopy for Q_1's f_{10}. (b) Spectroscopy for Q_1's f_{21}. (c) Spectroscopy for Q_1's f_{21}. Note that, in the spectroscopy experiment shown in (c), we insert a rectangular pulse which swaps the excitation between Q_1 and the bus resonator before the readout pulse. The black dash line indicates the frequency of the bus resonator. The avoided crossing whose separation reveals the coupling strength between the qubit and the resonator is observed.

S3 [3, 5–7].

READOUT CORRECTION

The fidelity matrix for calibrating the measured probabilities is defined as [3, 5–9]

$$\hat{F} = \begin{pmatrix} f_0 & e_{01} & e_{02} \\ e_{10} & f_1 & e_{12} \\ e_{20} & e_{21} & f_2 \end{pmatrix}, \tag{S47}$$

where f_j $(j = 0, 1, 2)$ is the probability that correctly gets the qubit's $|0\rangle$, $|1\rangle$ and $|2\rangle$ state by the measurement, e_{jk} $(j, k = 0, 1, 2)$ represents the errors describing the leakage probabilities from state $|k\rangle$ to $|j\rangle$. If we define $\hat{P}_m$ as the measured probabilities and $\hat{P}_i$ as the intrinsic probabilities for the system. The relation between $\hat{F}$, $\hat{P}_m$ and $\hat{P}_i$ is simply given by

$$\hat{P}_m = \hat{F} \cdot \hat{P}_i, \tag{S48}$$

which means the system's intrinsic states are reconstructed by making matrix inversion. The data used in our calibration is extracted from the measured I-Q values, as shown in FIG. S4.

NUMERICAL SIMULATION

Numerical simulations are performed to verify the experimental results. These simulations mainly consider two Hamiltonians, for Q_2-R and Q_1-R interaction, respectively, i.e.,

$$H_{Q_2R}/\hbar = \omega_{1,Q_2}|1\rangle\langle 1| + \omega_r a^+ a + g_2(a^+|0\rangle\langle 1| + a|1\rangle\langle 0|), \tag{S49}$$

$$H_{Q_1R}/\hbar = \omega_{1,Q_1}|1\rangle\langle 1| + \omega_{2,Q_1}|2\rangle\langle 2| + \omega_r a^+ a + \sqrt{2}g_1(a^+|1\rangle\langle 2| + a|2\rangle\langle 1|), \tag{S50}$$

where $\omega_{j,Q_j}/2\pi$ is the working frequency point for Q_j's $|j\rangle$ state, a and a^+ are the annihilation and creation operators for photons in the bus resonator, and $|k\rangle\langle l|$ is Q_j's jumping operator from state $|l\rangle$ to $|k\rangle$. Decoherence of Q_j and the bus resonator coupling to environment (consider a Markovian case for simplicity) is included by use of the Lindblad master equation

$$\dot{\rho} = -\frac{i}{\hbar}[H_{Q_jR}, \rho] + \frac{1}{T_r}\mathcal{D}[a]\rho + \frac{1}{T_{1,j}^{|1\rangle}}\mathcal{D}[b_j]\rho + \frac{1}{T_{\phi,j}^{|1\rangle}}\mathcal{D}[b_j^+ b_j]\rho, \tag{S51}$$

where a and b_j are the annihilation operators for the bus resonator and the qubit [10], respectively, the qubit dephasing rate is $1/T_{\phi,j}^{|1\rangle} = 1/T_{2,j}^{*,|1\rangle} - 1/2T_{1,j}^{|1\rangle}$, the Lindblad super-operator $\mathcal{D}[O]$ is defined as

$$\mathcal{D}[O]\rho = O\rho O^\dagger - \frac{1}{2}O^\dagger O\rho - \frac{1}{2}\rho O^\dagger O. \tag{S52}$$

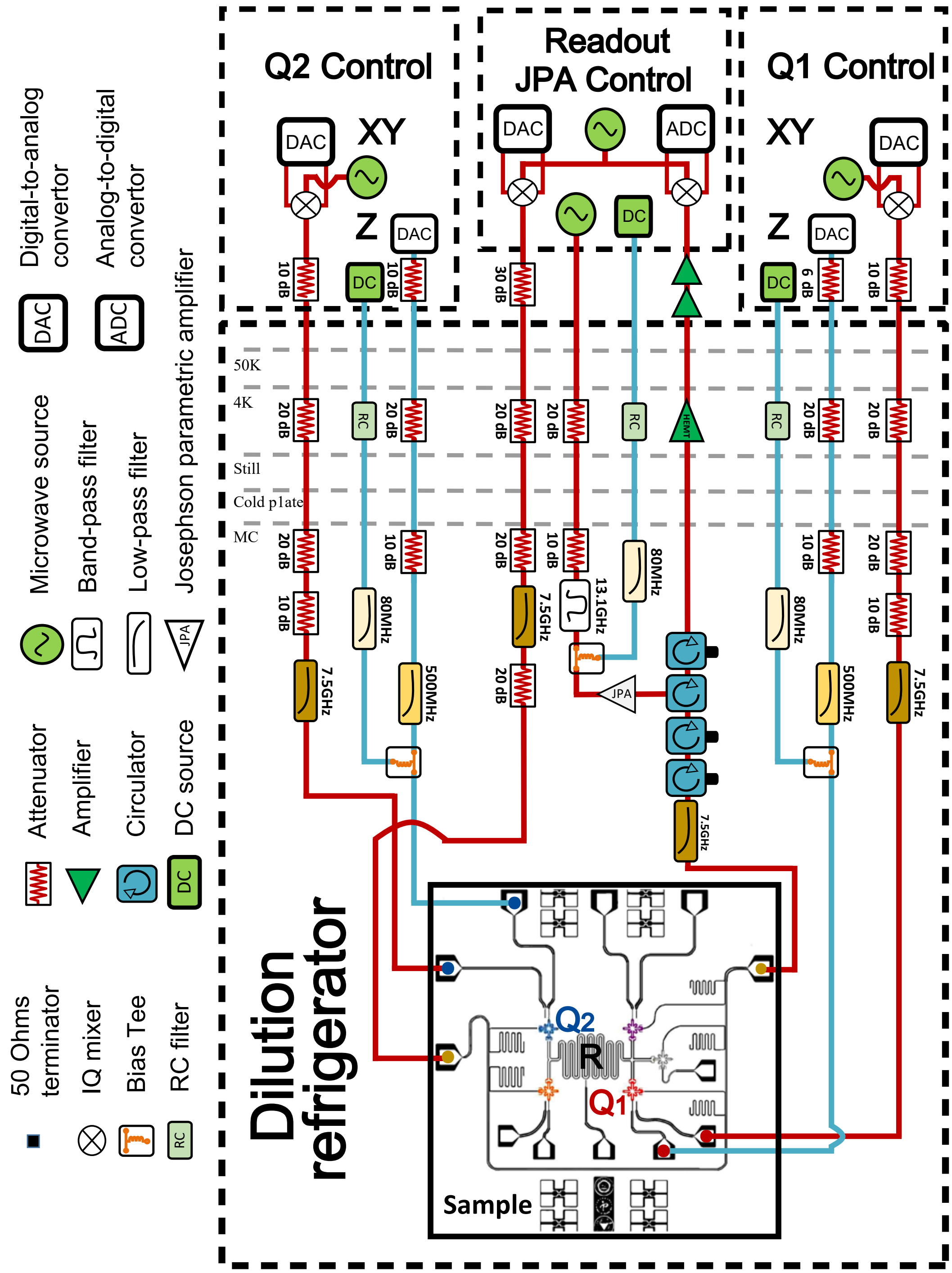

FIG. S3. Schematic lay out of the device and the experimental setup. The used superconducting circuit sample possesses five frequency-tunable Xmon qubits, two of which are used and labled as Q_1 and Q_2; all the qubits are coupled to a bus resonator R, which has a fixed bare frequency $\omega_r/2\pi = 5.582$ GHz; each qubit can be individually frequency-biased and frequency-modulated (through Z line) and flipped (through XY line), and has its own readout resonator assisting to produce its state information. Each qubit's XY control is implemented through the mixing of the low-frequency signals yielded by 2 Digital-to-analog converter (DAC)'s I/Q channels and a Microwave source (MS) whose carrier frequency is about 5.5 GHz; while the Z control is implemented by two signals: one is produced by the Direct-current (DC) biasing line from a low frequency DC source, the other is directly from the Z control of a DAC. The qubits' readout is implemented by the mixing of the signals of 2 DAC's I/Q channels and a MS with the frequency of about 6.6 GHz as to output a readout pulse with 2 tones targeting 2 qubits' readout resonators. The output from the sample, before being captured and demodulated by Analog-to-digital converter (ADC), is amplified sequentially by the impedance-transformed Josephson parametric amplifier (JPA, which is pumped by a MS with the frequency of about 13.5 GHz and modulated by a DC bias), high electron mobility transistor (HEMT) and room temperature amplifiers. Both the DAC and ADC are field programmable gate array (FPGA)-controlled to respond at the nanosecond scale. Furthermore, the custom-made circulators, attenuators and filters are added to the specific locations of the signal lines to reduce the noises affecting the operation of the device.

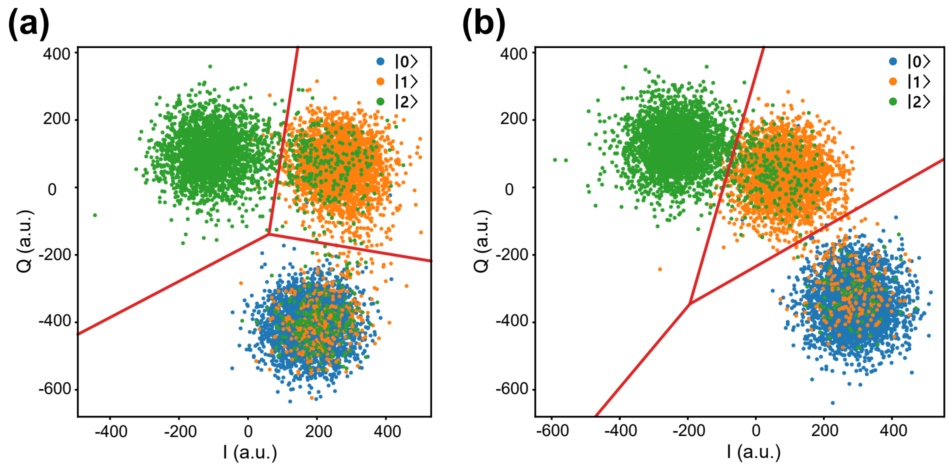

FIG. S4. The measured I-Q values when each qubit is prepared in $|0\rangle$ (blue), $|1\rangle$ (orange) and $|2\rangle$ (green) state. (a) The I-Q data of Q_1. (b) The I-Q data of qubit Q_2.

EXPERIMENTAL PULSE SEQUENCES

The pulse sequences for the experiment in the temporal order are shown in FIG. S5, which are roughly summed up to include three stages: the preparation of the specific superposition state for the resonator which acts as the WPD; the realization of a conditional phase gate for the resonator's photon state conditional on Q_1's $|1\rangle$ state; the readout of Q_1's state (FIG. S5(a)) and Q_1-Q_2's joint states (FIG. S5(b)), which are respectively used to reveal the Ramsey signals and characterize the qubit-WPD entanglement.

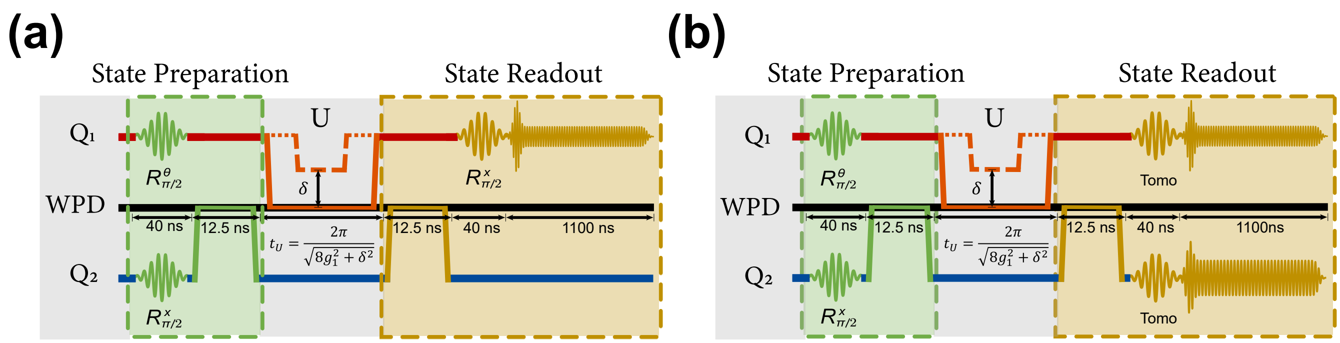

FIG. S5. Pulse sequence. (a) The pulse sequences for detecting the probability of Q_1 in $|1\rangle$ state. The creation of the WPD's state: (1) a microwave $\pi/2$-pulse $R^x_{\pi/2}$ prepares Q_2 in $(|0\rangle - i|1\rangle)/\sqrt{2}$ state; (2) a rectangular pulse then tunes Q_2 to the bus resonator (R)'s frequency to couple its $|0\rangle \leftrightarrow |1\rangle$ transition with R for a period of 12.5 ns before tuning it back to its idle frequency. The realization of a conditional phase gate operation U for the WPD: (1) a microwave $\pi/2$-pulse $R^\theta_{\pi/2}$ applied on Q_1 prepares it in $(|0\rangle - ie^{i\theta}|1\rangle)/\sqrt{2}$ state; (2) a rectangular pulse then tunes Q_1's $|1\rangle \leftrightarrow |2\rangle$ close to the bus resonator, realizing the U-transformation for the resonator's single photon state conditional on Q_1's $|1\rangle$ state; (3) a second microwave $\pi/2$-pulse $R^x_{\pi/2}$ applied on Q_1 transforming its $|0\rangle$ ($|1\rangle$) state to $(|0\rangle - i|1\rangle)/\sqrt{2}$ ($(|1\rangle - i|0\rangle)/\sqrt{2}$) state. The final step is the measurement of Q_1 to distinguish whether it is in $|1\rangle$ state, as to reveal the Ramsey signals. Before doing this measurement, the bus resonator state is mapped onto Q_2: a rectangular pulse tuning Q_2's $|0\rangle \leftrightarrow |1\rangle$ transition to the bus resonator's frequency for a period of 12.5 ns. (b) The pulse sequences for measuring the entanglement between Q_1 and the resonator. The difference to (a) is that the joint tomography of both qubits are performed, as to characterize the entanglement between Q_1 and the resonator.

Supplementary References

* These authors contributed equally to this work.
† zbyang@fzu.edu.cn
‡ yangcp@hznu.edu.cn
§ t96034@fzu.edu.cn

[1] W. K. Wootters, Entanglement of formation of an arbitrary state of two qubits, Phys. Rev. Lett. **80**, 2245 (1998).
[2] B.-G. Englert, Fringe visibility and which-way information: An inequality, Phys. Rev. Lett. **77**, 2154 (1996).
[3] C. Song, S.-B. Zheng, P. Zhang, K. Xu, L. Zhang, Q. Guo, W. Liu, D. Xu, H. Deng, K. Huang, D. Zheng, X. Zhu, and H. Wang, Continuous-variable geometric phase and its manipulation for quantum computation in a superconducting circuit, Nat. Commun. **8**, 1061 (2017).
[4] R. Barends, J. Kelly, A. Megrant, A. Veitia, D. Sank, E. Jeffrey, T. C. White, J. Mutus, A. G. Fowler, B. Campbell, Y. Chen, Z. Chen, B. Chiaro, A. Dunsworth, C. Neill, P. O'Malley, P. Roushan, A. Vainsencher, J. Wenner, A. N. Korotkov, A. N. Cleland, and J. M. Martinis, Superconducting quantum circuits at the surface code threshold for fault tolerance, Nature **508**, 500 (2014).
[5] W. Ning, X.-J. Huang, P.-R. Han, H. Li, H. Deng, Z.-B. Yang, Z.-R. Zhong, Y. Xia, K. Xu, D. Zheng, and S.-B. Zheng, Deterministic entanglement swapping in a superconducting circuit, Phys. Rev. Lett. **123**, 060502 (2019).
[6] Z.-B. Yang, P.-R. Han, X.-J. Huang, W. Ning, H. Li, K. Xu, D. Zheng, H. Fan, and S.-B. Zheng, Experimental demonstration of entanglement-enabled universal quantum cloning in a circuit, npj Quantum Inf. **7**, 44 (2021).
[7] K. Xu, W. Ning, X.-J. Huang, P.-R. Han, H. Li, Z.-B. Yang, D. Zheng, H. Fan, and S.-B. Zheng, Demonstration of a non-abelian geometric controlled-not gate in a superconducting circuit, Optica **8**, 972 (2021).
[8] C. Song, K. Xu, W. Liu, C.-p. Yang, S.-B. Zheng, H. Deng, Q. Xie, K. Huang, Q. Guo, L. Zhang, P. Zhang, D. Xu, D. Zheng, X. Zhu, H. Wang, Y.-A. Chen, C.-Y. Lu, S. Han, and J.-W. Pan, 10-qubit entanglement and parallel logic operations with a superconducting circuit, Phys. Rev. Lett. **119**, 180511 (2017).
[9] Y. Zheng, C. Song, M.-C. Chen, B. Xia, W. Liu, Q. Guo, L. Zhang, D. Xu, H. Deng, K. Huang, Y. Wu, Z. Yan, D. Zheng, L. Lu, J.-W. Pan, H. Wang, C.-Y. Lu, and X. Zhu, Solving systems of linear equations with a superconducting quantum processor, Phys. Rev. Lett. **118**, 210504 (2017).
[10] R. Barends, J. Kelly, A. Megrant, D. Sank, E. Jeffrey, Y. Chen, Y. Yin, B. Chiaro, J. Mutus, C. Neill, P. O'Malley, P. Roushan, J. Wenner, T. C. White, A. N. Cleland, and J. M. Martinis, Coherent josephson qubit suitable for scalable quantum integrated circuits, Phys. Rev. Lett. **111**, 080502 (2013).